Chlorine-trapped CVD bilayer graphene for resistive pressure sensor with high detection limit and high sensitivity

2017 2D Mater. 4 025049

(http://iopscience.iop.org/2053-1583/4/2/025049)

2D Materials

PAPER

RECEIVED
7 December 2016

REVISED
21 February 2017

ACCEPTED FOR PUBLICATION
28 February 2017

PUBLISHED
17 March 2017

Chlorine-trapped CVD bilayer graphene for resistive pressure sensor with high detection limit and high sensitivity

Viet Phuong Pham[1,2,4], Minh Triet Nguyen[2,4], Jin Woo Park[2], Sung Soo Kwak[2], Dieu Hien Thi Nguyen[2], Mu Kyeom Mun[2], Hoang Danh Phan[3], Doo San Kim[2], Ki Hyun Kim[2], Nae-Eung Lee[1,2] and Geun Young Yeom[1,2]

[1] SKKU Advanced Institute of Nano Technology (SAINT), Sungkyunkwan University (SKKU), Suwon, Gyeonggi-do 440-746, Korea
[2] School of Advanced Materials Science and Engineering, SKKU, Suwon, Gyeonggi-do 440-746, Korea
[3] Department of Mechanical Engineering, SKKU, Suwon, 440-746, Korea
[4] Both authors contributed equally to this work.

E-mail: nelee@skku.edu **and** gyyeom@skku.edu

Keywords: ZnO nanorods, Cl-trapped graphene pressure sensor, bilayer graphene, pre-doping, Cl radical doping

Supplementary material for this article is available online

Abstract

Pressure sensing is one of the key functions for smart electronics. Considerably more effort is required to achieve the fabrication of pressure sensors that can imitate and overcome the sophisticated pressure sensing characteristics in nature and industry, especially in the innovation of materials and structures. Almost all of the pressure sensors reported until now have a high sensitivity at a low-pressure detection limit (<10 kPa). While the exploration of a pressure sensor with a high sensitivity and a high responsivity at a high-pressure is challenging, it is required for next generation smart electronics. Here, we report an exotic heterostructure pressure sensor based on ZnO/chlorine radical-trap doped bilayer graphene (ZGClG) as an ideal channel for pressure sensors. Using this ZGClG as the channel, this study shows the possibility of forming a pressure sensor with a high sensitivity (0.19 kPa^{-1}) and a high responsivity (0.575 s) at $V = 1$ V on glass substrate. Further, the pressure detection limit of this device was as high as 98 kPa. The investigation of the sensing mechanism under pressure has revealed that the significant improved sensing effect is related to the heavy p-type chlorine trap doping in the channel graphene with chlorine radicals without damaging the graphene. This work indicates that the ZGClG channel used for the pressure sensing device could also provide a simple and essential sensing platform for chemical-, medical-, and biological-sensing for future smart electronics.

Introduction

High sensitivity, high detection limit, and low cost are highly desired for the coming generations of sensor devices. Particularly, pressure sensing is one of the key functions for smart electronics. In general, there are three types of pressure sensors: resistive, capacitance, and piezoelectric [1–10]. Among these, the resistive sensor is a conventional pressure sensing type that transduces the pressure imposed on the sensor to resistance signals. It has been widely utilized due to its attractive advantages including ease of fabrication, low price, and facile signal collection [9, 11–13]. The pressure sensing range and sensitivity limit are two of the most important factors used to judge the pressure sensing performance of pressure sensors. Most of the pressure sensors reported until now have high sensitivities at a low-pressure detection limit (<10 kPa) [1–6]. Pressure sensors with high sensitivity and high responsivity at the high-pressure detection limit have not been explored and need investigation and understanding.

Graphene, a zero band gap semiconductor with an atomically single layer (SL) thickness, has been known to be a very promising sensing platform for detecting the individual molecules leading to the ultimate sensitivity for gas sensors [14–19], pressure sensors [20–22], photodetectors [23], bio-sensors [24, 25], strain sensors [26, 27], and temperature sensors [28, 29]. Unfortunately, these devices based on graphene have shown a medium level sensitivity which is not sufficient for various practical applications. Therefore, to solve this sensitivity limit problem, a hybrid structure composed of graphene layers and a number of compatible semiconductors have been investigated. Recently, graphene-based semiconductor hybrid nanostructures have received considerable

attention for use in optoelectronic devices, photocatalysts, water splitting devices, and sensor devices [30–37]. Among the compatible semiconductors, ZnO has been investigated as one of the best because of its large bandgap (3.37 eV) and high binding energy (60 MeV) [38]. Graphene/ZnO nanorod (NR) hybrid structures have been fabricated via chemical vapor deposition (CVD), seeded solution growth, chemical conversion method, and polymer substrate transferring [30–36, 39]. Graphene/ZnO NR hybrid structures have also been obtained by the reduction of graphene oxide (GO) after the formation of a GO/ZnO NRs hybrid structure due to the poor conductivity of GO [40, 41].

Doping is an outstanding strategy for increasing the conductivity, mobility, and sensitivity of 2D materials. For example, doping on graphene has been successfully demonstrated for gas sensing such as NO_2 and NH_3 gas detection by boron doped graphene [15], H_2S gas detection by Fe doped graphene [16], CO gas detection by nitrogen doped graphene [17], SO_2 gas detection by Al doped graphene [18], and formaldehyde detection by boron, nitrogen, and sulfur doped graphene [19]. Although the exploration and development of new doping species are still progressing, they remain challenging. Chemical doping on graphene is an effective strategy in electrical tuning and band-gap engineering; unfortunately, it has a low stability and some residue remains on the graphene surface, which induces degradation in devices [42–52]. For example, HNO_3 and $AuCl_3$ have been utilized as possible p-type dopants on graphene for reducing sheet resistance (R_s) [43–52]. However, they involve various unresolved problems. For example, HNO_3 is evaporated in ambiance from the graphene surface due to its high volatility, which induces a gradual reduction of electrical conductivity of the devices [43–48, 50–52]. In addition, $AuCl_3$ leaves ~100 nm Au particles on the graphene surface, which reduces the performance, decreases the stability, and increases the leakage current of the devices [43, 45–48].

Among various doping methods, plasma doping is a potentially effective dry-doping technique which has not been explored sufficiently for tuning graphene properties. Zhang *et al* utilized microwave plasma with DC biasing for the Cl functionalization of graphene, whereby well-controlled Cl coverage on graphene (~45.3%) was achieved [53]. Cl plasma doping is one of the best-controlled graphene doping methods [54]. Cl doping on graphene surface has been successfully simulated by density functional theory (DFT) in previous reports [55, 56], with results showing the opening of a direct bandgap energy of 1.21 eV. Thereby, plasma doping induces the reduction of R_s without the degradation of optical transmittance [57]. However, in conventional plasma doping approaches, the reduction of R_s by plasma exposure is limited because the bombardment by energetic ion particles induces damage to the graphene network.

A wide-range of Cl absorption on graphene surfaces using Cl_2 inductively coupled plasma (ICP) sources has been recently reported by Marinov *et al* [58]. In this study, we propose an outstanding strategy utilizing Cl dry doping on CVD graphene by Cl radicals directly on fresh graphene/Cu foil both before transfer (pre-doping) and after transfer (normal doping) to the substrate; therefore, trapping Cl atoms between the two graphene layers. Cl radicals were obtained by using a remote plasma-type radio frequency-ICP (RF-ICP) source with a dual mesh grid [59–62]. Using the Cl radical trapped graphene layers, a pressure sensor with a hybrid channel based on a ZnO NRs/2nd CVD graphene layer/trapped Cl radical doping/1st CVD graphene layer (ZnO/G/Cl/G) was fabricated. By using this novel strategy, a ZGClG pressure sensor with the high conductivity, high-pressure detection limit (98 kPa), high responsivity (0.575 s), and high sensitivity (0.19 kPa^{-1}) could be achieved. Through the graphene/ZnO NR hybrid structure platform with highly conductive Cl radical trapped graphene layers, it is believed that new flexible and stretchable electronics with high loading pressure and high sensitivity could be realized for future pressure research fields such as e-skin.

Results and discussion

Figure 1(A) shows a pressure-sensing device fabrication sequence that is based on the hybrid channel of ZnO/G/Cl/G (figure S1-supplementary information) (stacks.iop.org/TDM/4/025049/mmedia). First, the 1st graphene layer was doped using Cl radicals by pre-doping and normal doping (fresh graphene/Cu foil was doped using Cl radicals before the wet transfer (pre-doping) to a glass substrate, and the transferred 1st graphene layer was further doped after the wet transfer (normal doping)) to increase the Cl atom coverage on the transferred 1st graphene layer surface. The doped 1st graphene layer was covered with an additional 2nd graphene layer to form the Cl trap-doped bilayer graphene (BLG) and the Cl-trap doped BLG was then used as a channel of a pressure sensing device. By using the Cl trap-doped BLG, Cl dopants adsorbed on the graphene layers could be kept without loss between the graphene layers under ambient environments (heat, moisture, O_2, etc) as reported by previous researches [59, 60]. In addition, in conventional plasma doping, graphene is generally damaged by breaking the C–C bonding in the graphene (the C–C bond strength of graphene is very delicate at 4.9 eV) due to the high energy ion bombardment during the plasma exposure [63]. In our strategy, for Cl radical doping without damaging the graphene surface, we installed a double mesh-grid in a 13.56 MHz RF-ICP system (figure S2-supplementary information) to remove ion bombardment during Cl radical doping, which is the key factor in breaking a graphene lattice structure. After the Cl trap-doped BLG was annealed in a vacuum at 230–250 °C (figure S3-supplementary information) for 30 min–3 h [59, 60, 62], the Ti/Au electrodes were deposited as source/drain. Next, tetratetracontate

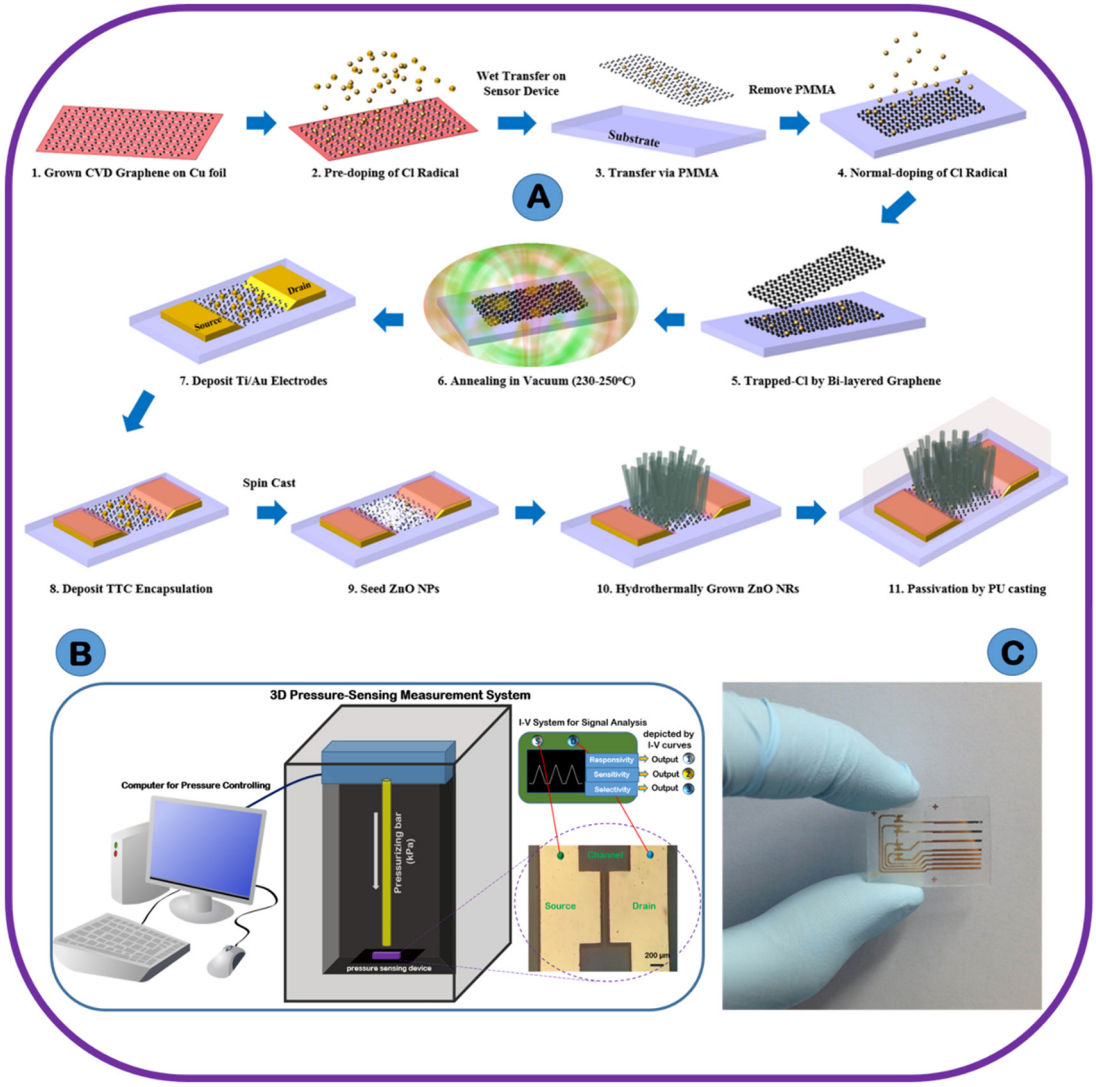

Figure 1. (A) Fabrication sequence of a highly sensitive and homogeneous pressure-sensing device based on the hybrid channel of ZnO NRs/2nd graphene layer/trapped Cl atoms/1st graphene layer. (B) Schematic diagram of the pressure-sensing measurement system. Inset: optical microscopic image of Ti/Au electrodes and ZnO NRs/2nd graphene layer/trapped Cl atoms/1st graphene layer channel in the sensor (channel). (C) A photograph of the fabricated pressure sensor device.

(TTC) or SiO_2 powder was selectively deposited as a thin encapsulation layer using a shadow mask on top of source-drain Ti/Au electrodes to prevent the growth of ZnO NRs on the electrodes. The ZnO NRs were then grown on the graphene layer to form a pressure sensor device with the ZGClG channel and the device was passivated using polyurethane (PU). Finally, these pressure sensor devices were tested at 300 K using the pressure test equipment shown in figure 1(B), which is connected to the current–voltage (I–V) measurement system measuring the device output signals. The inset in figure 1(B) shows the optical microscopic image of Ti/Au electrodes (source/drain) and the ZnO NRs/2nd graphene layer/ trapped Cl atoms/1st graphene layer (ZGClG) channel for the pressure sensor device. Figure 1(C) shows the photograph of the completed pressure sensor structure. In the Supporting Information (figure S4-supplementary information), the optical transparency of the pressure sensors at visible light range is shown and, using ZGClG channel, the optical transparency of about 72.9% on glass substrate could be achieved. It is recently reported that almost no change of pressure sensor characteristics by UV light irradiation during pressurizing [64, 65].

To investigate the trapping effect of Cl radical atoms between the 1st and 2nd graphene layer for the Cl-trapped BLG, the water droplet contact angle images and TEM images were captured based on bright field (BF), diffraction pattern (DP), dark field (DF), and scanning transmission electron microscopy electron energy loss spectroscopy (STEM_EELS) of BLGs (figure S5 and S6-supplementary information). Figure S6(A) (supplementary information) shows BF-, DP-, DF-TEM, and STEM_EELS images of an intrinsic BLG without the presence of Cl atoms, except for the locations in the thin line network (thin black line network in BF and white line network in DF). Slight Cl doping in the thin network is believed to be due to the $FeCl_3$ etchant utilized during the etching of Cu from graphene/Cu foil, as investigated in previous reports

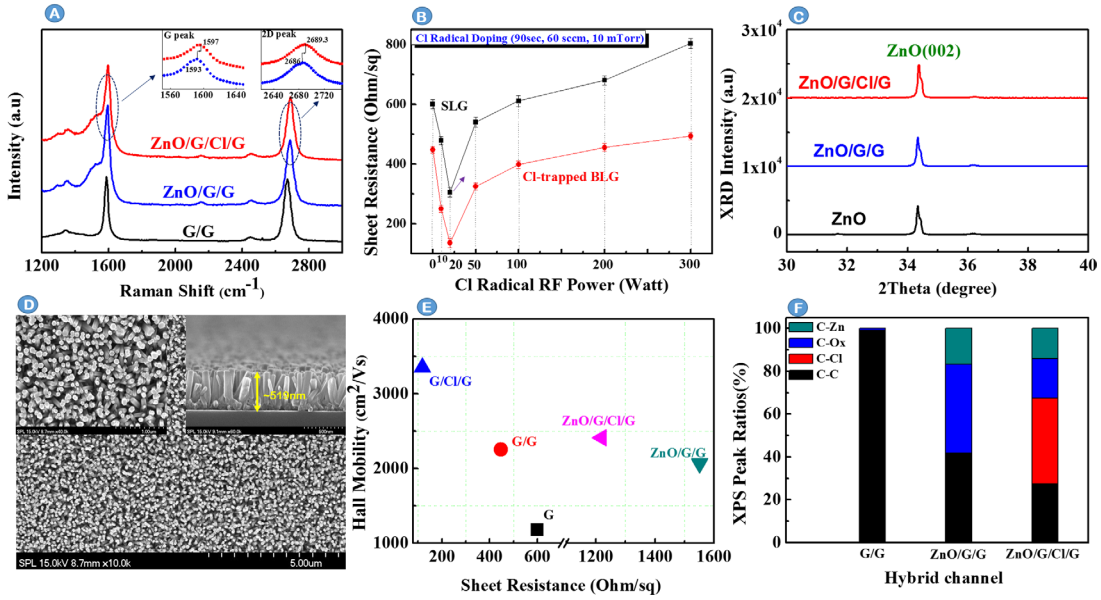

Figure 2. (A) Raman spectra of G/G, ZnO/G/G, and ZnO/G/Cl/G (ZGClG) channels. Inset: Raman blue shifts of the D and 2D peaks of ZGClG compared to those of ZnO/G/G. (B) R_s of SLG and BLG as a function of RF power (0 W (pristine) ~ 300 W) of ICP source for Cl radical doping. (C) XRD spectra of ZnO (0 0 2) peak for ZnO, ZnO/G/G, and ZGClG channels. (D) SEM images of ZnO NRs grown on glass substrate (5 μm scale bar). Left-inset: SEM image of ZnO NRs at a higher magnification (1 μm scale bar), right-inset: cross-section SEM image of the height of ZnO NRs at a higher magnification (500 nm scale bar). (E) Hall mobilities as a function of R_s for hybrid channels of G (SLG), G/G (BLG), G/Cl/G (Cl trap-doped BLG), ZnO/G/G (ZnO on pristine BLG), and ZGClG (ZnO on Cl trap-doped BLG). (F) Peak intensity ratios of each component in C 1*s* XPS spectra for G/G, ZnO/G/G, and ZGClG hybrid channels.

[59, 60]. However, for the Cl-trapped BLG, as can be seen in the BF and DF as cloud shapes in Region 1 and Region 2 of figure S6(B) (supplementary information), regions of the Cl atom were observed between the two graphene layers, indicating the presence of trapped Cl atoms between the BLGs. The existence of Cl atom clouds was also confirmed through the micro-EDS of TEM in previous reports [59, 60]. Moreover, the high thermal stability (at 230 C in vacuum for 100 h), high mechanical stability (1400 bending cycles), and high chemical stability (in air (120 d), DI water and acetone) of Cl-radical trap doping in graphene at low energy has been well investigated by Pham *et al* [59].

For further investigation, in figure S7 (supplementary information), the work functions of four cases with/without Cl doping were measured: single layer graphene (SLG), Cl doped-SLG, BLG, and Cl-trapped BLG by Ultraviolet Photoelectron Spectroscopy (UPS). The result showed the work functions of 4.86, 6.22, 5.41, and 6.46 eV, for SLG, Cl doped-SLG, BLG, and Cl-trapped BLG, respectively. Therefore, the Cl trap-doped BLG (after vacuum annealing) showed the highest work function (6.46 eV), which is higher than that previously reported (4.321 and 4.462 eV of HNO_3-doped BLGs) [43, 44]. It is believed that the highest work function observed for the Cl trap-doped BLG is due to the heavy p-type dry trap doping of Cl atoms as observed in the TEM of figure S6(B) (supplementary information) compared with the work function of previous wet doping methods using HNO_3, $AuCl_3$ [43, 44].

To further understand the Cl radical doping effect, Raman analysis was carried out. Figure 2(A) shows the Raman analysis for the device hybrid channels composed of pristine BLG (G/G), ZnO grown on the pristine BLG (ZnO/G/G), and ZnO grown on Cl trap-doped BLG (ZnO/G/Cl/G; ZGClG). The Raman spectra showed the disorder of the defect peak (D peak) near 1350 cm^{-1} for the channels of ZnO/G/G and ZGClG due to the growth of the ZnO NRs on the graphene surface possibly caused by the increased binding of Zn with carbon during the growth of ZnO NRs on graphene. In addition, the zoom-in Raman spectra of the G (near 1600 cm^{-1}) and 2D (near 2700 cm^{-1}) peaks showed the blue shift for ZGClG compared with ZnO/G/G due to the heavy p-type doping with Cl atoms (Inset of figure 2(A)), indicating the existence of the Cl doping effect due to Cl trapping between the graphene layers, even after the growth of the ZnO NRs in a wet solution.

For the investigation of the optimized RF plasma power for the Cl radical doping on graphene surface, the sheet resistance R_s was measured as a function of RF power to the ICP source (0 W (pristine) ~ 300 W) for SLG and BLG (Cl trap-doped and annealed at 230–250 °C). The results are shown in figure 2(B). The Cl radical doping time was maintained at 90 s. In the case of SLG, the lowest R_s value of about 305 Ω/sq was obtained at 20 W, while at the higher power values, the R_s monotonically increased with the increase of RF power due to the damage on the graphene network induced by ion bombardment from the high power chlorine plasma. In the case of BLG, the lowest value of R_s of 118 Ω/sq could also be obtained at 20 W, similar to SLG. In addition, the further increase of RF power also increased the R_s due to the damage on the graphene

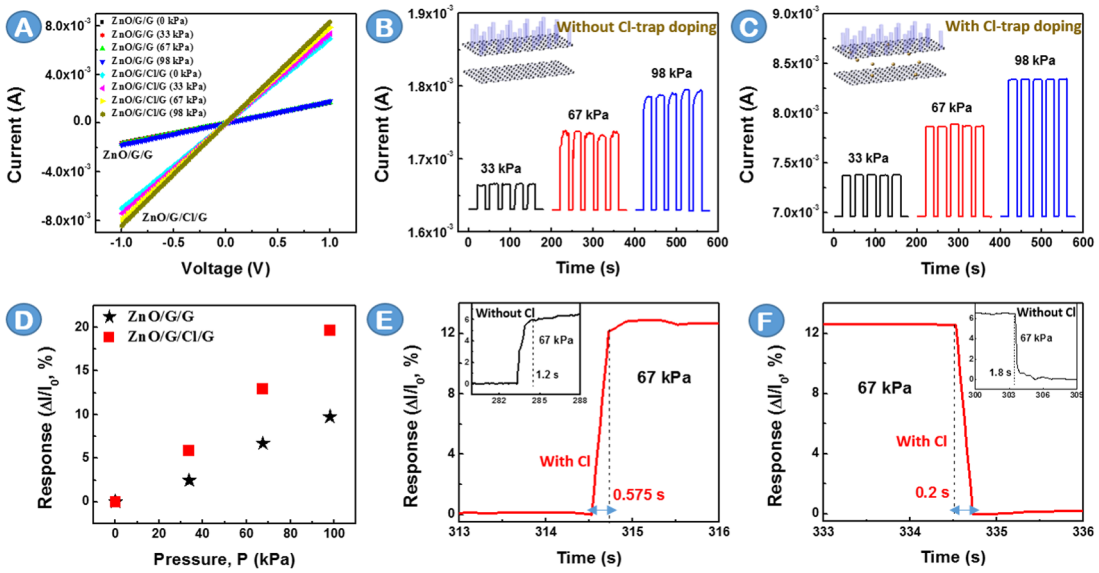

Figure 3. (A) Change of current (I_{DS}) between two electrodes through the channel in the device shown in figure 1, measured as a function of applied voltage (V) for the hybrid channels such as ZnO/G/G and ZGClG. (B) and (C) Dependence of current with time for the ZnO/G/G channel and the ZGClG channel, respectively, while repeatedly pressing for 10 s with different pressures. (D) Current responses of the devices with ZnO/G/G and ZGClG hybrid channels for different pressures applied to the devices. (E) and (F) Current responses of the ZGClG channel measured as a function of time for pressure-on and pressure-off, respectively. In the insets, those of the ZnO/G/G channel are also shown. As the pressure, 67 kPa was used.

surface. The increased damage on the graphene surface with the increase of RF power is related to penetration of energetic ions through dual mesh system at higher RF powers.

The crystallinity and structure of the ZnO NRs grown on the graphene surface were investigated using x-ray diffraction (XRD) for ZnO, ZnO/G/G, and ZGClG, the result of which is shown in figure 2(C). The XRD spectra showed a strong peak at $2\theta = \sim 34.38°$ attributed to the ZnO (002) crystal plane for all the samples, indicating the perfectly vertical growth of the ZnO NRs on graphene surfaces [66, 67]. In addition, the XRD spectra revealed that the peaks have the half maximum width value of ~0.19°, which implies the high quality crystallinity of the ZnO NRs. For the morphological observation of ZnO NRs grown on the graphene surface (i.e. on ZnO/G/G and ZGClG), ZnO images grown on graphene/glass substrate were observed using scanning electron microscopy (SEM) and atomic force microscopy (AFM) (figure 2(D) and figure S8-supplementary information, respectively). The SEM image (scale bar of 5 μm) in figure 2(D) shows the uniform and vertically grown ZnO NRs with the average diameter of ~100 nm (left-inset) and the average height of ~519 nm (right-inset). The inset of figure 2(D) shows the SEM image of ZnO NRs at the scale bar of 1 μm. In general, the vertically and uniformly grown ZnO NRs would significantly improve the pressure-sensing performance compared with the less vertically and non-uniformly grown ZnO NRs [68].

Figure 2(E) shows the Hall carrier mobility measured using the Hall effect measurement as a function of R_s for various channel layers such as SLG, BLG, G/Cl/G, ZnO/G/G, and ZGClG. Here, the Hall carrier concentration showed a value of ~10^{12} cm^{-2} for Cl-doped samples composed of G/Cl/G, ZnO/G/G, and ZGClG. The graphene was Cl doped at the optimized power of 20 W for 90 s. The results showed 1176 cm^2 V^{-1} s^{-1} (600 Ω/sq) for SLG, 2252 cm^2 V^{-1} s^{-1} (447 Ω/sq) for BLG, 3352 cm^2 V^{-1} s^{-1} (118 Ω/sq) for G/Cl/G, 2067 cm^2 V^{-1} s^{-1} (1551 Ω/sq) for ZnO/G/G, and 2411 cm^2 V^{-1} s^{-1} (1229 Ω/sq) for ZGClG. Therefore, the channel layers with chlorine trap doped graphene (i.e. G/Cl/G versus G/G and ZGClG versus ZnO/G/G) exhibited higher Hall mobility in addition to the lower R_s. The chemical bonding between carbon in graphene and other elements (C1s) was also investigated for G/G, ZnO/G/G, and ZGClG using x-ray photoelectron spectroscopy (XPS) and the results are shown in figure 2(F) and table S1 (supplementary information). The chemical bindings of carbon with other elements were C–Cl, C–C, C–O_x, and C–Zn. After the ZnO growth on the G/G surface, bindings related to C–Zn and C–O_x were observed. Also, for the ZnO growth on the G/Cl/G surface, a significant portion of carbon in graphene was bonded to chlorine in addition to C–Zn and C–O_x, indicating the chlorine trap doping effect. Using XPS, the element peaks of O 1s (~532 eV), Zn 2p (~1022 eV), C 1s (~284.6 eV), and Cl 2p (~200.8 eV) could also be identified for ZGClG (figure S9-supporting information).

Figure 3(A) shows the change of the current (I_{DS}) between two electrodes through the channel in the device shown in figure 1, measured as a function of applied voltage (V) for the hybrid channels such as ZnO/G/G and ZGClG. The voltage bias was swept from −1 to 1 V and both samples were measured at 300°K. As shown, at the same pressure, the current for

the device with the ZGClG channel was higher than that with the ZnO/G/G channel by showing 9mA of I_{DS} for the ZGClG channel compared with 2mA of I_{DS} for the ZnO/G/G channel at 1 V. Figures 3(B) and (C) show the dependence of I_{DS} with time for the ZnO/G/G channel and the ZGClG channel, respectively, while repeatedly pressing for 10 s with different pressures. As shown, after the devices were pressed, the I_{DS} values increased and became saturated (for the pressure of 33, 67, and 98 kPa, the saturated I_{DS} values were 1.66, 1.73, and 1.78 mA, respectively, for the ZnO/G/G channel and 7.38, 7.87, and 8.33 mA, respectively, for the ZGClG channel). In addition, as the pressure was removed, the I_{DS} values recovered to the baseline for both devices. Moreover, the current baseline was not changed during the repeated pressing, indicating that both devices were stable in the pressure measurement. In this pressure sensor, we pressurized our sensor devices until 5 cycles, and there was no base-line shift, no degradation, or no hysteresis effect in stability of our device could be found.

The power consumption of our pressure sensor device is $P \sim 7$ mW. This is a reasonable value, although it is not the lowest comparing with previous reports [69]. Still, the constructing of resistive pressure sensor with very low consumption is desiring and challenging issue. Recent reports revealed some potential solutions to solve for this hot issue such as (i) developing the self-powered sensing devices which represents a significant step forward for achieving sustainability in pressure sensors [70–73], or (ii) combining the sensing components with energy generation units such as organic solar cell and thermoelectric device, then self-powered pressure sensors might run continuously without the external power supply [70], (iii) hybridization of the energy generation process and the sensing process into only one self-powered pressure sensor that has been achieved by piezoelectric and triboelectric pressure sensors [70], or (iv) an organic thermoelectric material based pressure sensor, which can use the energy generated from the applied temperature of the device, may as another novel candidate for self-powered sensing application [70]. All above strategies are quite expected to produce ultra-low power consumption for resistive pressure sensors.

Figure 3(D) shows the current responses of the devices for different pressures applied to the devices. The current response is defined by the difference of current between the initial state and the excited state; it is calculated by the formula $\frac{\Delta I}{I_0} = \frac{I - I_0}{I_0}$ (%), where I and I_0 are the current response and the current baseline, respectively. Both devices exhibited higher current response at the higher pressure and the device with the ZGClG channel showed higher current response than the device with the ZnO/G/G channel. That is, for the pressures of 33, 67, and 98 kPa, the current responses of the device with the ZnO/G/G channel were 2.45%, 6.69%, and 9.75%, respectively, while those of the device with the ZGClG channel were 5.89%, 12.93%, and 19.68%, respectively. Therefore, the pressure sensitivities of the devices with the ZnO/G/G channel and the ZGClG channel, which are calculated from the slope between the y-axis (current response, $\frac{\Delta I}{I_0}$) and x-axis (pressure values, P) values were 0.09 and 0.19 kPa^{-1}, respectively. For these devices, the highest pressure loaded to the devices in this study was 98 kPa due to the stability of the devices. For these devices, the highest pressure loaded to the devices in this study was 98 kPa. Under a higher pressure (>98 kPa), our ZnO NRs could be bended and it is hard to recover back the initial state, leading instability of performance output. So, it is noted that, for the higher pressure operation, the ZGClG configuration should be optimized on flexible or stretchable platforms to spread the force directly on entire sample in the future.

In figures 3(E) and (F), the current responses of the ZGClG channel measured as a function of time are shown for pressure-on and pressure-off, respectively. In the insets, those of the ZnO/G/G channel are also shown. As the pressure, 67 kPa was used. As shown, the currents were almost instantly increased to the saturated value and decreased to the baseline as the devices were pressurized and unpressurized, respectively. As shown in figure 3(E), the response time for the pressure-on, which is defined as $\Delta t_1 = t - t_0$, where t is the time to reach the current saturation and t_0 is the time at the current baseline, was calculated as 0.575 s for the ZGClG channel and 1.2 s for the ZnO/G/G channel. The response time in the case of pressure-off, which is defined as $t_2 = t_0 - t$, was 0.2 s for the ZGClG channel compared with 1.8 s for the ZnO/G/G channel, as shown in figure 3(F). In general, for all of the pressures investigated, the device with the ZGClG channel exhibited higher performance than that of the device with the ZnO/G/G channel such as higher sensitivity and faster response time.

For the possible explanation of the above results, schematic diagrams of the pressure sensing mechanism for the devices are shown in figures 4(A)–(F). After ZnO NRs and graphene surface make contact, a very small depletion can form near the contact area in the graphene, similar to a p-n junction, because ZnO NR is an n-type material and the graphene is a p-type material. Since the work functions of Cl-trapped BLG, ϕ_{Gr}, and the electron affinity of ZnO, χ_{ZnO}, are 6.46 eV (figure S7-supplementary information) and 4.3 eV, respectively, the Fermi level of Cl-trapped BLG is shifted toward the conduction band by electron transferred from n-type ZnO to Cl-trapped BLG. Also, the Fermi level of ZnO is also aligned to balance at the interface (figure 4(E)). In the depletion zone, the positive piezoelectric polarization ions of ZnO NRs, which are non-mobile charges, result in temporarily trapping of minority carriers of electron from graphene. Therefore, it causes the holes in graphene are accumulated near the interfaces by p-n contact, leading electrons in the ZnO accumulated at the bottom of the ZnO NRs (figure 4(A)). This results in a vertical electric field direction from bottom to top between the

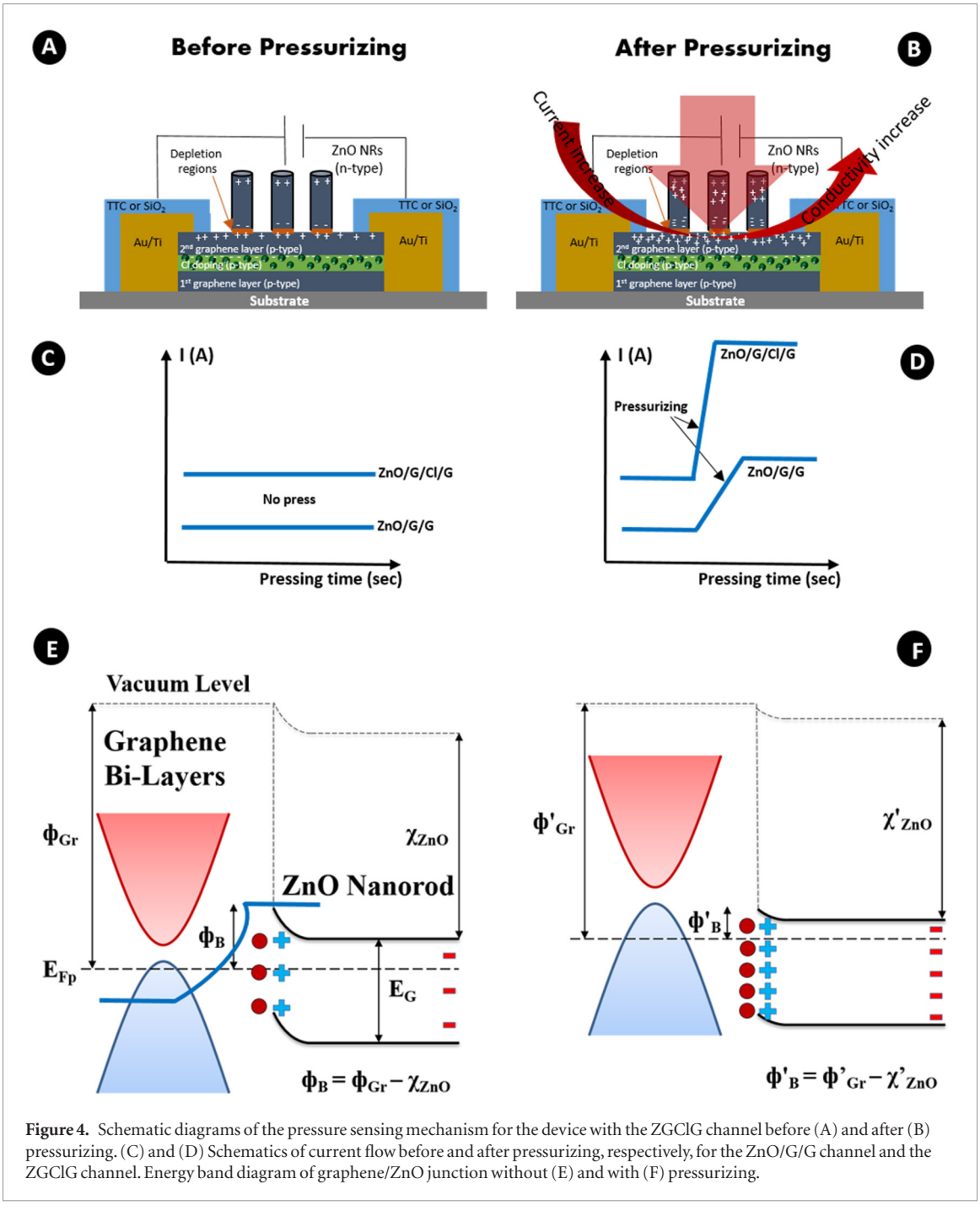

Figure 4. Schematic diagrams of the pressure sensing mechanism for the device with the ZGClG channel before (A) and after (B) pressurizing. (C) and (D) Schematics of current flow before and after pressurizing, respectively, for the ZnO/G/G channel and the ZGClG channel. Energy band diagram of graphene/ZnO junction without (E) and with (F) pressurizing.

ZnO NRs and graphene. For the ZGClG channel, due to the high electronegativity of chlorine, the Cl atoms between the graphene capture electrons from both graphene layers by the Cl-trap doping between the two layers of graphene, and create extra holes at the interface (figure 4(A)). Therefore, during the period no pressure, the current of the ZGClG channel is higher than that of the ZnO/G/G channel at a given voltage (figure 4(C)), as shown in figure 3(A). By loading a pressure vertical to the graphene onto the top of the device, more holes are accumulated in the 1st and 2nd graphene layer, meanwhile, the ZnO NRs are affected by stress and polarized inside. Therefore, by applying pressure to the device, the polarization charges of ZnO NRs are increased and it leads more electron attraction from Cl-trapped BLG. The increased positive piezoelectric charges may effectively result in lowering barrier height, ϕ_B, between graphene and ZnO NRs at the interface [74, 75], and in turn, more electrons easily transferring to ZnO NRs from graphene, leading to create a new aligned Fermi level after pressurization (figure 4(F)). Also, the accumulation of hole is increased and consequently the current is increasesd due to the increased conductance of the channel during pressing. For the ZGClG channel, the Cl atoms trapped between the graphene layers bond more tightly with the graphene layers by compressing the Cl-trapped BLG; therefore, further holes are injected into the graphene layers during pressing in addition to the extra holes injected into the 2nd layer graphene, leading to higher polarization of ZnO NRs (figure 4(B)). Therefore, as shown in figure 4(D), while the device is undergoing pressurization, the current

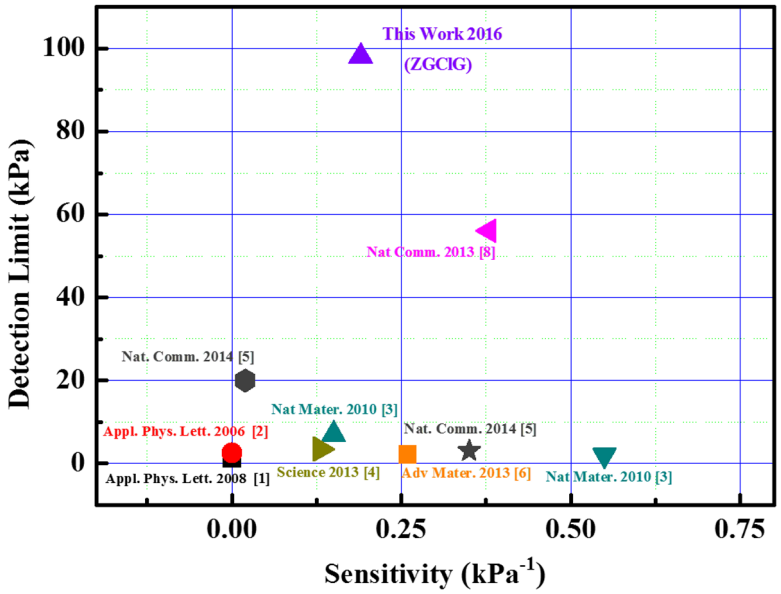

Figure 5. Performance comparison of the ZGClG pressure sensor in this work with other reported pressure sensors.

increases more rapidly and the flow of current increases for the ZGClG channel compared to the ZnO/G/G channel. In addition, for Cl-radical trapping, Cl itself does not create a gap between two layers of graphene. It just shows a trapping effect between the top graphene layer and the bottom graphene layer for forming the C–Cl bonding which is revealed in figure S5 and S6, and table S1 (supporting information) in order to increase the conductivity and the sensitivity of pressure sensor devices.

Two parameters are involved with the pressure sensors, sensitivity and detection limit, which are critical to the efficient operation of the pressure sensor. The detection limit is the ability to push a force onto the device. The detection limit versus pressure sensitivity of the most recent pressure sensor devices investigated including the current device with the ZGClG channel is shown in figure 5. Here, the devices located in the right hand side corner show higher sensitivity, while the devices located in the left hand side corner show a higher pressure detection range. Our pressure senor device with the ZGClG channel not only exhibited high sensitivity but also a high detection limit. The outstanding detection limit of our device is attributed to the dense ZnO NRs on the graphene. By increasing the number of ZnO NRs on the surface, the force is spread on the rods and is uniformly transmitted to the graphene layers. Therefore, the maximum detection pressure is limited by the material nature and device structure investigated in our work. The pressure sensing characteristics of the most recently proposed pressure sensors, including our devices, are also shown in table S2 (supplementary information). In table S2, the pressure sensing characteristics of the devices with the ZGClG channel and those with the ZnO/G/G channel are also shown. As can be seen, by using the Cl-trapped BLG as the graphene channel instead of the pristine BLG channel, not only higher sensitivity but also faster response time was obtained due to the increased conductivity of the Cl-trapped BLG during pressurizing. As a result, as shown in figure 5 and table S2 (supplementary information), considering the sensitivity as well as the sensing range of the most recently proposed pressure sensing devices investigated, our ZGClG pressure sensors are one of the best pressure sensing devices investigated [1–9].

Conclusions

A pressure sensor device with the ZGClG channel having high detection limit and high responsivity was successfully fabricated. By using the Cl radical trap-doped BLG as the channel graphene for the pressure sensing channel, a pressure sensor device with high sensitivity (0.19 kPa^{-1}) and high responsivity (0.575 s) was achieved while pressurizing the device at 300°K at V ~1 V. In contrast, the pressure sensor device with the ZnO/G/G which does not have Cl doping between the graphene layers showed lower sensitivity (0.09 kPa^{-1}) and lower responsivity (1.2 s) at 300 °K at V ~1 V. The improved sensitivity and responsivity of the device with the Cl-trap doped BLG channel (ZGClG channel) instead of the pristine BLG channel (ZnO/G/G channel) was due to the increased conductivity of the channel by the injection of extra hole carries to the graphene during the pressurizing of the Cl-trap doped BLG channel. The pressure sensor device investigated in this study also showed a high pressure detection limit of 98 kPa, possibly due to the dense ZnO NRs on the graphene which spread the force, which was then uniformly transmitted to the graphene layers. This work indicates that the resistive pressure sensing device with the ZGClG channel, that is, the use of the Cl-trapped BLG channel, significantly enhances the device characteristics to detect high pressure with a high sensitivity. Therefore, it is believed that the Cl-trap doped BLG channel could be utilized as an essential

sensing platform for next-generation chemical-, medical-, and biological-sensing devices in addition to the pressure-sensing devices which are integrated into future smart electronics such as health monitoring [71].

Experimental methods

Synthesis of the graphene layer

Fresh single layer graphene (SLG) was grown on Cu via chemical vapor deposition (CVD) method. Cu foil with the area of 10 × 8 cm^2 and the thickness of 75 μm was rolled into a CVD vacuum chamber made of quartz. First, the CVD chamber was filled with H_2 gas at a flow rate of 10 sccm, and the Cu foil was annealed for 1 h at the temperature of 1050 °C in the H_2 environment. Next, graphene was synthesized at 1050 °C by flowing H_2/CH_4 (10/20 sccm) for 30 min, and after that, the chamber was cooled down to room temperature with H_2 gas (10 sccm) for 1 h. After the synthesis, the Cu foil was cut into small equally-sized pieces (3 × 3 cm^2). These small pieces of graphene/Cu foil were then affixed on glass substrates using a tape. The glass substrates were used as holders for the graphene-Cu foil assembly.

Maximization strategy for Cl-trapping between graphene layers

For wet transfer of 2nd graphene in the deionized (DI) water to the substrate with the 1st graphene doped with Cl, to minimize the removal of the adsorbed Cl dopants on the doped 1st graphene surface during the transfer, the substrate with Cl doped 1st graphene was not directly dipped in the DI water during the graphene transfer. Instead, to transfer 2nd graphene on the substrate with the Cl doped 1st graphene, we used a polyethylene terephthalate (PET) film to pick up the edge of poly(methyl methacrylate) (PMMA)-coated 2nd graphene in the DI water and transferred on the already Cl doped 1st graphene while minimizing the removal of dopants on the 1st graphene during the wet transfer process.

Trap-doping by Cl radical absorption and post-annealing sequence

First, Cl radical doping was carried out on fresh graphene/Cu foil as pre-doping before the wet transfer to a glass substrate for higher Cl atom coverage on the graphene surface. After the wet transfer to the glass substrate, the pre-doped 1st graphene-coated glass substrate was further doped by normal doping using the same Cl radical doping condition. The pre- and normal doped 1st graphene-coated glass substrate was covered with a 2nd graphene layer to trap the Cl dopants between the graphene layers. The Cl radical doping was conducted using an ICP system with a double mesh grid (to prevent ion bombardment on the graphene surface by blocking energetic ion transmission through the grids) at 10 mTorr 60 sccm Cl_2 and at 20 W of 13.56 MHz RF power (figure S2-supplementary information) [59–62]. The pre- and normal Cl radical doping time was maintained at 90 s. Finally, the Cl-trap doped BLG on glass substrates was annealed in vacuum at 230–250 °C for 30 min–3 h (figure S3-supplementary information).

Preparation of ZnO solution and growth of ZnO NRs on BLG

A butyl acetate solution with 40 wt% ZnO nanoparticles (NPs) was purchased from Sigma Aldrich. The size of the ZnO NPs ranged from 35 to 100 nm. A 5 wt% solution was prepared by diluting the 40 wt% butyl acetate solution. A seed layer of ZnO NPs was formed by drop-casting ZnO NPs on the BLGs (BLGs with and without Cl-trap doping) and was dried at 130 °C for 5 min. To coat ZnO NPs selectively on the BLG surface, avoiding the Ti/Au electrodes of the pressure sensor device, TTC or SiO_2 powder was selectively deposited on the electrodes using a shadow mask. Next, 0.025 M of zinc nitrate hexahydrate ($Zn(NO_3)_2 \cdot 6H_2O$) and hexamethylenetetramine (HTMA) was dispersed in 200 ml H_2O for 2 h at 300°K to form a ZnO solution. In addition, ZnO NRs were grown on the BLG coated with ZnO NPs by a hydrothermal method in the ZnO solution at 90 °C for 2 h. Finally, PU was coated using a spin coating method on the device with the ZnO grown graphene channel and the device was heated at 120 °C for 2 h for encapsulation. The encapsulated PU film significantly improved the adhesion between the ZnO NRs and the BLG host materials (BLGs with and without Cl-trap doping) and protected the ZnO NRs from contamination and corrosion. Also, the encapsulated PU forced the ZnO NRs to deform elastically and uniformly to minimize physical damage under various pressure forces.

Fabrication of pressure sensor device

The pressure sensor devices with the ZnO/G/Cl/G (ZGClG) channel and with the ZnO/G/G channel were manufactured on glass substrate. Before processing the Cl trap-doped BLG and pristine BLG on the glass substrates as described in the previous section, the BLGs (BLGs with and without Cl-trap doping) were annealed at 140 °C for 2 h to eliminate the interaction between the graphene and adsorbed water to remove any electrical instability. Next, Ti/Au (10/50 nm) electrodes were formed on the BLGs by thermal evaporation using a shadow mask. Then, as a thin encapsulation layer, TTC (by using a shadow mask) or 200 nm thick SiO_2 powder (by thermal evaporation) was coated selectively on the top of the Ti/Au electrodes using a shadow mask by thermal evaporation to prevent the growth of ZnO NRs during the ZnO growth on the BLG surface. Finally, PU was coated on the device using a spin coating method.

Characterization

R_s of the graphene films on the glass substrate (or SiO_2 wafer) was measured using a R_s meter (Dasoleng, FPP-2400) at 300°K. UV–vis spectra (Shimadzu, 3600) was used for optical transmittance of the sensor devices.

Raman spectra (Renishaw, RM-1000 Invia) with the excitation energy of 2.41 eV (514 nm, Ar^+ ion laser) was used for the characterization of the graphene films doped with the Cl radicals. Chemical composition of the graphene channel was characterized utilizing x-ray photoelectron spectroscopy (XPS, ESCA2000, VG Microtech. Inc.) with a Mg Kα twin-anode source and with the take-off angle of 45°. C 1*s*, O 1*s*, Zn 2*p*, and Cl2p peak intensities and their binding states between C with C, Zn, Cl, and O_x were measured. Optical microscope (OM, Olympus-BX51M) was used to observe the morphology of the devices. The contact angle measure equipment (Dataphysics, OCA 15EC, Spain) are used to observe the morphology of the sensor devices. Field emission-scanning electron microscope (FE-SEM, Hitachi S-4700) was used to observe the morphology of the devices. To observe Cl atom locations between the graphene layers for a Cl-trap doped bilayer graphene, Transmission Electron Microscopy (TEM, FEI Titan 80/300) with the bright field (BF), dark field (DF), and diffraction pattern (DP), micro-EDS (energy dispersive x-ray spectroscopy) installed in the TEM, and scanning transmission electron microscopy-electron energy loss spectroscopy (STEM-EELS) were utilized. X-ray diffractometer (XRD, Ultima IV) was utilized to observe the ZnO NRs structure on the devices. Atomic force microscopes (AFM, Bruker Innova Microscope) was used to measure the surface roughness of ZnO NRs grown on the device channels. Hall effect measurement system (HMS-3000, ECOPIA) was used to characterize the carrier mobility and hole concentration of the sensor devices. Work Functions (Φ_M) of doped and undoped graphene layers were measured by Ultraviolet Photoelectron Spectroscopy (UPS) using the 4B1 beam line located at the Pohang accelerator laboratory, POSTECH, Korea. Pressure measurement system (Pushing Tester-ZPS-100, Junil Tech. Co.) was used to investigate the pressure sensing limit and sensitivity of the fabricated sensor devices that are connected directly to a current–voltage (*I–V*) measurement system.

Acknowledgments

V P Pham and M T Nguyen contributed equally to this work. V P Pham and M T Nguyen thank S-W Kim for assistance of pressure sensing measure equipment, and thank K S Kim for fixing the ICP equipment. This research was supported by Nano Material Technology Development Program through the National Research Foundation of Korea (NRF), funded by the Ministry of Education, Science, and Technology (2016M3A7B4910429).

References

[1] Metzger C, Fleisch E, Meyer J, Dansachmuller M, Graz I, Kaltenbrunner M, Keplinger C, Schwodiauer R and Bauer S 2009 *Appl. Phys. Lett.* **92** 013506
[2] Manunza I, Sulis A and Bonfiglio A 2006 *Appl. Phys. Lett.* **89** 143502
[3] Mannsfeld S C B, Tee B C K, Stollenberg R M, Chen C V H H, Barman S, Muir B V O, Sokoloz A N, Reese C and Bao Z 2010 *Nat. Mater.* **9** 859
[4] Wu W Z, Wen X N and Wang Z L 2013 *Science* **340** 952
[5] Pan L, Chortos A, Yu G, Wang Y, Isaacson S, Allen R, Shi Y, Dauskardt R and Bao Z 2014 *Nat. Commun.* **5** 3002
[6] Yao H B, Ge J, Wang C F, Wang X, Hu W, Zheng Z J, Ni Y and Yu S H 2013 *Adv. Mater.* **25** 6692
[7] Lee H K, Chang S and Yoon E 2006 *J. Microelectromech. Syst.* **15** 1681
[8] Schwartz G, Tee B C K, Mei J, Appleton A L, Kim D H, Wang H and Bao Z 2013 *Nat. Commun.* **4** 1859
[9] Shirinov A V and Schomburg W K 2008 *Sensors Actuators* A **142** 48
[10] Smith A D *et al* 2013 *Nano Lett.* **13** 3237
[11] Lee I and Sung H J 1999 *Exp. Fluids* **26** 27
[12] King M G, Baragwanath A J, Rosamond M C, Wood D and Gallant A J 2009 *Proc. Chem.* **1** 568
[13] Fraden J 2010 *Handbook of Modern Sensors, Physics, Designs, and Applications* 4th edn (New York: Springer)
[14] Schedin F, Geim A K, Morozov S V, Hill E W, Blake P, Katsnelson M I and Novoselov K S 2007 *Nat. Mater.* **6** 652
[15] Lv R *et al* 2015 *PNAS* **112** 14527
[16] Zhang H, Luo X, Song H, Lin X, Lu X and Tang Y 2014 *Appl. Surf. Sci.* **317** 511
[17] Ma C, Shao X and Cao D 2014 *Sci. China Chem.* **57** 911
[18] Liu X Y, Zhang J M, Xu K W and Ji V 2014 *Appl. Surf. Sci.* **313** 405
[19] Zhou Q, Yuan L, Yang X, Fu Z, Tang Y, Wang C and Zhang H 2014 *Chem. Phys.* **440** 80
[20] Xu Y, Guo Z, Chen H, Yuan Y, Lou J, Lin X, Gao H, Chen H and Yu B 2011 *Appl. Phys. Lett.* **99** 133109
[21] Sorkin V and Zhang Y W 2011 *J. Mol. Model.* **17** 2825
[22] Trung T Q and Lee N E 2016 *Adv. Mater.* **28** 4338
[23] Liu C H, Chang Y C, Norris T B and Zhong Z 2014 *Nat. Nanotechnol.* **9** 273
[24] Kim D J, Sohn I Y, Jung J H, Yoon O J, Lee N E and Park J S 2013 *Biosens. Bioelectron.* **41** 621
[25] Jung J H, Sohn I Y, Kim D J, Kim B Y, Jang M and Lee N E 2013 *Carbon* **62** 312
[26] Trung T Q, Tien N T, Kim D, Jang M, Yoon O J and Lee N E 2014 *Adv. Funct. Mater.* **24** 117
[27] Hempel M, Nezich D, Kong J and Hofmann M 2012 *Nano Lett.* **12** 5714
[28] Trung T Q, Tien N T, Kim D, Jung J H, Yoon O J and Lee N E 2012 *Adv. Mater.* **24** 5254
[29] Sahoo S, Barik S K, Sharma G L, Khurana G, Scott J F and Katiyar R S 2012 arXiv: 1204.1928
[30] Chen J, Li C, Eda G, Zhang Y, Lei W, Chhowalla M, Milne W I and Deng W Q 2011 *Chem. Commun.* **47** 6084
[31] Kim M K, Yi D K and Paik U 2010 *Langmuir* **26** 7552
[32] Lee J M, Pyun Y B, Yi J, Choung J W and Park W I 2009 *J. Phys. Chem.* C **113** 19134
[33] Chen Z, Zhang N and Xu Y J 2013 *Cryst. Eng. Commun.* **15** 3022
[34] Zhang N, Zhang Y and Xu Y J 2012 *Nanoscale* **4** 5792
[35] Zhang N, Yang M Q, Tang Z R and Xu Y J 2014 *ACS Nano* **8** 623
[36] Chang H, Sun Z, Ho K Y F, Tao X, Yan F, Kwok W M and Zheng Z 2011 *Nanoscale* **3** 258
[37] Xiang Q, Yu J and Jaroniec M 2012 *Chem. Soc. Rev.* **41** 782
[38] Wang Z L 2004 *J. Phys.: Condens. Matter* **16** R829
[39] Choi D *et al* 2010 *Adv. Mater.* **22** 2187
[40] Yin Z, Wu S, Zhou X, Huang X, Zhang Q, Boey F and Zhang H 2010 *Small* **6** 307
[41] Alver U, Zhou W, Belay A B, Krueger R, Davis K O and Hickman N S 2012 *Appl. Surf. Sci.* **258** 3109
[42] Liu H, Liu Y and Zhu D 2011 *J. Mater. Chem.* **21** 3335
[43] Han T H, Lee Y, Choi M R, Woo S H, Bae H H, Hong B H, Ahn J H and Lee T W 2012 *Nat. Photonics* **6** 105
[44] Bae S *et al* 2010 *Nat. Nanotechnol.* **5** 574
[45] Park M H, Han T H, Kim Y H, Jeong S H, Lee Y, Cho H and Lee T W 2015 *J. Photon. Energy* **5** 053599
[46] Xu W, Lim T S, Seo H K, Min S Y, Cho H, Park M H, Kim Y H and Lee T W 2014 *Small* **10** 1999

[47] Xu W, Seo H K, Min S Y, Cho H, Lim T S, Oh C Y, Lee Y and Lee T W 2014 *Adv. Mater.* **26** 3459
[48] Xu W, Wang L, Liu Y, Thomas S, Seo H K, Kim K I, Kim K S and Lee T W 2015 *Adv. Mater.* **27** 1619
[49] Kasry A, Kuroda M A, Martyna G J, Tulevski G S and Bol A A 2010 *ACS Nano* **4** 3839
[50] Gunes F, Shin H J, Biswas C, Han G H, Kim E S, Chae S J, Choi J Y and Lee Y H 2010 *ACS Nano* **4** 4595
[51] Liu Z, Li J, Sun Z H, Tai G, Lau S P and Yan F 2012 *ACS Nano* **6** 810
[52] Kim Y, Ryu J, Park M, Kim E S, Yoo J M, Park J, Kang J H and Hong B H 2014 *ACS Nano* **8** 868
[53] Zhang X, Hsu A, Wang H, Song Y, Kong J, Dresselhaus M S and Palacios T 2013 *ACS Nano* **7** 7262
[54] Wu J, Xie L, Li Y G, Wang H L, Ouyang Y, Guo J and Dai H 2011 *J. Am. Chem. Soc.* **3** 19668
[55] Sahin H and Ciraci S 2012 *J. Phys. Chem.* C **116** 24075
[56] Yang M, Zhou L, Wang J and Liu Z 2012 *J. Phys. Chem.* C **116** 844
[57] Lim Y D, Lee D Y, Shen T Z, Ra C H, Choi J Y and Yoo W J 2012 *ACS Nano* **6** 4410
[58] Marinov D, Foucher M, Campbell E, Brouard M, Chabert P and Booth J P 2016 *Plasma Sources Sci. Technol.* **25** 035019
[59] Pham V P, Kim K N, Jeon M H, Kim K S and Yeom G Y 2014 *Nanoscale* **6** 15301
[60] Kim K N, Pham V P and Yeom G Y 2015 *ECS J. Solid State SC* **4** N5095
[61] Pham V P, Kim K H, Jeon M H, Lee S H, Kim K N and Yeom G Y 2015 *Carbon* **95** 664
[62] Pham V P, Kim D S, Kim K S, Park J W, Yang K C, Lee S H and Yeom G Y 2016 *Sci. Adv. Mater.* **8** 884
[63] Brenner D W, Shenderova O A, Harrison J A, Sttuart J S, Ni B and Sinnott S B 2002 *J. Phys. Condens. Matter* **14** 783
[64] Sun Q, Kim D H, Park S S, Lee N Y, Zhang Y, Lee J H, Cho K and Cho J H 2014 *Adv. Mater.* **26** 4735
[65] Jung H, Chun S, Kim Y, Oh H S, Bae G Y, Bae G and Park W 2015 *J. Nanosci. Nanotechnol.* **15** 9020
[66] Lee H S, Man M T, Park K D, Oh H M, Kim J, Jeong H, Kim Y H and Jeong M S 2015 *J. Korean Phys. Soc.* **67** 1819
[67] Jung M H and Lee H 2011 *Nanoscale Res. Lett.* **6** 159
[68] Shin D M, Tsege E L, Kang S H, Seung W, Kim S W, Kim H K, Hong S W and Hwang Y H 2015 *Nano Energy* **12** 268
[69] Gong S, Schwalb W, Wang Y, Chen Y, Tang Y, Si J, Shirinzadeh B and Cheng W 2014 *Nat. Commun.* **5** 3132
[70] Zang Y, Zhang F, Di C A and Zhu D 2015 *Mater. Horiz.* **2** 140
[71] Zhang L, Hou G, Wu Z and Shanov V 2016 *Nano Life* **6** 1642005
[72] Lin L, Xie Y, Wang S, Wu W, Niu S, Wen X and Wang Z L 2013 *ACS Nano* **7** 8266
[73] Xu S, Qin Y, Xu C, Wei Y, Yang R and Wang Z L 2010 *Nat. Nanotechnol.* **5** 366
[74] Wang Z L 2012 *MRS Bull.* **37** 814
[75] Wu W, Pan C, Zhang Y, Wen X and Wang Z L 2013 *Nano Today* **8** 619